Grafting of alpha-tocopheryl phosphate on chemically treated Ti-6Al-4V for antibacterial bone implants

Applied Surface Science 619 (2023) 156681

Contents lists available at ScienceDirect

Applied Surface Science

journal homepage: www.elsevier.com/locate/apsusc

Full Length Article

Grafting of alpha-tocopheryl phosphate on chemically treated Ti-6Al-4V for antibacterial bone implants

Francesca Gamna [a,*], Amanda M. Wiecek [a], Andrea Cochis [b], Jacopo Barberi [a], Alessandro C. Scalia [b], Lia Rimondini [b], Silvia Spriano [a]

[a] Applied Science and Technology Department, Politecnico di Torino, C. so Duca degli Abruzzi 24, Torino 10129, Italy
[b] Department of Health Sciences, Center for Translational Research on Autoimmune and Allergic Diseases – CAAD, Università Del Piemonte Orientale UPO, Corso Trieste 15/A, Novara (NO), 28100, Italy

ARTICLE INFO

Keywords:
Alpha tocopheryl phosphate
Titanium
Nanocoating
Antibacterial
Bone

ABSTRACT

Alpha-tocopheryl phosphate (α-TP) is the water-soluble form of the antioxidant and lipophilic molecule alpha-tocopherol. Even if α-TP's antioxidant and antibacterial properties are known, it has never been exploited to prevent implantable materials against bacterial surface contamination, till now. Accordingly, the purpose of this work is to couple a chemically treated Ti6Al4V surface with α-TP conferring a local antibacterial activity preserving orthopaedic and dental prosthetic devices. The grafting of the α-TP molecule is explored both as a thin coating (<0.2 μm thick) and through molecular functionalization. As a result, a homogeneous and continuous coating is obtained by auto-polymerization of the molecule on the treated titanium surface, as shown by reflectance spectroscopy, ζ potential titration curve, and Kelvin Prove assay. The coating exposes the phosphate groups (demonstrated by XPS and FTIR analysis), which give to the surface a hydrophilic (contact angle of 40° with water) and very effective antibacterial behaviour, thus reducing the surface infection from the pathogen *Staphylococcus epidermidis* of >3 logs (≈ 92%) in comparison to the uncoated controls. Contrarily, the phosphorylated groups were used to create the binding to the surface on the functionalized samples, as shown by the XPS analysis. The functionalized surface results in poor antibacterial properties (≈1 log reduction of viable colonies) and hydrophobic behaviour. Finally, the cytocompatibility evaluation towards human mesenchymal stem cells showed the coating treatment to be more cell's friendly in comparison with the functionalization.

1. Introduction

Biomaterials play an important role in orthopaedic and dental implant applications. Pure titanium and its alloys are the most used materials for permanent implants in contact with bone thanks to their fatigue resistance, low elastic modulus, stable chemical properties, and good biocompatibility [1] However, problems such as aseptic loosening and *peri*-implant microbial infection may lead to implant failure. The typical way of treating infections is antibiotic therapy through oral administration, which can often lead to the development of antibiotic-resistant bacteria and thus be ineffective, especially if bacteria are able to evolve in the biofilm form [2,3]. The term "biofilm" indicates a bacteria aggregate attached to a surface which is typically the cause of chronic and medical device-related infections from a clinical perspective. Because of the antibiotic-resistant nature of biofilms, the use of antibiotics alone is ineffective in treating biofilm-related infections [4,5] That is why scientific research today is working hard to find solutions to render titanium surfaces antibacterial through a local activity of non-antibiotic molecules. Several strategies have been studied to prevent infection by implementing surface modifications on titanium and using different antibacterial agents such as biomolecules, polymers, and metals [6,7,8–14]. In addition to this, new frontiers of titanium implants have been directed not only to fighting bacterial infection, but also to improving bioactivity and osseointegration, creating multifunctional surfaces that can simultaneously have a number of specific responses in tissues, cells, and bacteria [15] The biological role and benefits of vitamin E were considered and studied by the scientific community when its excellent antioxidant properties were discovered [16]. Indeed, alpha-tocopherol, one of the most abundant and biologically active isoforms of vitamin E, functions as the most effective lipid-soluble antioxidant [17]. In addition to its antioxidant capabilities, other properties, such as antibacterial and anti-inflammatory actions, are still

* Corresponding author.
E-mail address: francesca.gamna@polito.it (F. Gamna).

https://doi.org/10.1016/j.apsusc.2023.156681
Received 20 December 2022; Received in revised form 25 January 2023; Accepted 4 February 2023
Available online 15 February 2023

being studied [18–22]. The scientific community has increased its interest in this compound in recent years bringing the most compelling results in drug delivery systems, surface coatings, tissue engineering, and regeneration, and wound healing [23–28]. The antioxidant ability of this molecule can be conferred to materials and biomaterials to which it is coupled, but its hydrophobic nature makes difficult its use on surfaces devoted to direct and permanent contact with bone [28]. Over the past few decades, a water-soluble form of vitamin E, the alpha-tocopheryl phosphate (α-TP), has gained interest especially after it was naturally found in the plasma and tissues of humans and animals [29]. The OH chromanol group, typical of alpha-tocopherol, is phosphorylated to form α-TP thus losing its antioxidant property, but turning out to be a hydrophilic molecule, soluble in water, with -PO_4^{2-} functional groups exposed. α-TP is being studied for its antibacterial, osteogenic, and angiogenic properties, but there are still very few studies on its functionalization on solid surfaces and its effects [29–32]. In particular, the antibacterial effect of alpha tocopherol phosphate is still under study, and its mechanism of action is still not well understood. Only a few papers studying the antibacterial effect of phosphate can be found in the literature, claiming a good antibacterial effect toward *S. aureus* and *S. epidermidis* [30,33]. Based on these considerations, the purpose of this work is to develop a multifunctional surface by coupling a chemically treated Ti6Al4V surface with pro-osteogenic properties with a molecule, α-TP, with antibacterial properties for orthopedic and dental devices. The surface obtained after the chemical treatment displays both micro- and nano-roughness (Ra = 0.25 μm), and exposes acidic OH groups that allow not only pro-osteogenic properties but make the substrate suitable for grafting with biomolecules [34]. In this paper, two different strategies of surface grafting, molecular functionalization, and thin coating, are explored, and for both modes, the divalent Ca^{2+} ion is exploited as a linker between the surface, rich in deprotonated OH groups, and the α-TP molecule, which is also negatively charged in solution. This process was designed based on past studies from the Authors that used Ca^{2+} to ensure a bond between the above surface and gallic acid or polyphenols, which easily release H_3O^+ ions in solution [35].

Finally, different characterizations were carried out to evaluate the grafting of the α-TP molecule on the surface by means of different physical/chemical techniques such as contact angle, ζ potential, X-ray photoelectron spectroscopy (XPS), UV\Vis spectroscopy, FTIR analysis, and Kelvin probe force microscopy. The biological characterization was performed by cellular assays with human mesenchymal stem cells (hMSC), to evaluate the cytocompatibility, whereas the antibacterial activity was assessed by evaluating the ability of the coated or functionalized specimens to prevent the surface colonization of the pathogen *Staphylococcus epidermidis*.

2. Materials and methods

2.1. Surface chemical treatment

Ti6Al4V discs of 10 mm diameter and 2 mm thickness were used as substrates. First, the samples were polished with sandpaper (up to 400 grit). All samples were washed for 5 min in acetone and twice for 10 min in ultrapure water in an ultrasonic bath. A patented thermochemical treatment was done on the samples, consisting of an initial acid attack with dilute hydrofluoric acid (HF) to remove the native oxide layer and create a micro-and nano-rough surface, and then controlled oxidation with hydrogen peroxide [36]. These samples will be referred to as CT (chemically treated), while the samples polished up to 400 grit used as control will be denominated as mirror polished (MP).

2.2. Sample preparation for the functionalization or coating

First of all, the treated samples were irradiated with UV light for 1 h. Immediately after irradiation, the samples were immersed in a solution of $CaCl_2$ (0.292 g/L) for 24 h, minimizing sample contact with the air during the transfer. Alpha-tocopheryl phosphate (α-TP) ((±)-α-Tocopheryl phosphate disodium salt, T2020, Sigma-Aldrich, St. Louis, MO, USA) was employed for surface functionalization. For the grafting of the molecule, a solution of α-TP in TRIS-HCL with a concentration of 5 mg/mL was prepared by shaking the solution on a magnetic stirrer for 10 min, until the molecule was completely dissolved. After 24 h, the samples immersed in the calcium solution were dried under a laminar flow hood and then immersed in the prepared α-TP solution for 3 h at 37 °C.

2.2.1. Coating

The coating method involved the following steps. Firstly, the samples taken from the solution (see 2.2) were dried for 5 min under a laminar flow hood, in this way, the molecule can form a continuous layer adhered on the substrate. After the layer was dried, the samples were rinsed 3 times in ultrapure water, to remove the what was not adsorbed. Lastly, samples were dried again under a laminar flow hood.

2.2.2. Functionalization

The functionalization method involved the following steps. Firstly, the samples taken from the solution (see 2.2) were immediately rinsed 3 times in ultrapure water, precisely with the aim of avoiding the formation of a coating and allowing grafting of a molecular layer. Lastly, samples were dried under a laminar flow hood.

2.3. UV–Vis diffuse reflectance spectroscopy

Reflectance spectroscopy (R%) was carried out on solid samples (CT, CT_coating, CT_fun) in the range of 190–750 nm by equipping the spectrophotometer (UV-2600i, UV-2700i – Shimadzu) with the integrating sphere. The measurement was performed in reflectance mode with a slit width of 5 nm and a sampling interval of 1 nm. Barium sulphate (BaSO4) was used as a blank for baseline correction.

2.4. Kelvin probe force microscopy

This is a dual-scan system in which both a topographic image and a surface potential image are obtained by a forward scan in tapping mode and a backward scan in lift mode applying a bias between the tip and the sample. To achieve this type of measurement, the atomic force microscope (Innova atomic force microscope, Bruker) was equipped with a conductive tip (Sb-doped Si, frequency 75 kHz, SCM-PIT-V2, Bruker). For this analysis, specifically created samples were prepared as here described. The steps described in 2.1 and 2.2 were applied, then half of the sample was coated with Kapton® and the samples were coated or functionalized according to the procedure described in 2.2.1 or 2.2.2. After complete drying, the Kapton® was removed. The samples thus obtained were only half coated or functionalized with a rather narrow border with the other half of the sample. The final topography and potential images (100 × 100 μm) were acquired on the boundary between the functionalized and nonfunctionalized surface. The scanning parameters (scan frequency, lift height, tip-sample bias) were adjusted each time for the best results. Gwyddion software [37] was used to elaborate the images: a second-degree polynomial filter was applied to the topographical images while a matching filter was implemented for the potential images.

2.5. Fourier transform infrared spectroscopy (FTIR)

All sample surfaces (CT, CT_coating, CT_fun) were analyzed by Fourier transform infrared spectroscopy (FTIR, FTIR Hyperion 2000 – Tensor 27, Bruker Optics, Ettlingen, Germany) in ATR mode and compared with the spectrum of a drop of a solution of α-TP in water (concentration: 0,1 mg/ml). Spectra were acquired between 400 and 4000 cm^{-1} with a resolution of 4 cm^{-1} and 32 scans per measurement.

2.6. ζ potential titration curves

Surface zeta potential as a function of pH was analyzed by electrokinetic measurements (SurPASS, Anton Paar) on the three samples (CT, CT_coating, and CT_fun), equipped with an adjustable gap cell. The ζ potential was determined as a function of pH in an electrolyte solution of 0.001 M KCl, with a conductivity around 15 mS/m, and the pH value was varied by adding 0.05 M HCl or 0.05 M NaOH using the titration unit of the instrument. Separate couples of samples were used for the acidic and basic titrations in order to avoid artifacts due to surface reactions during the measurement.

2.7. X-ray photoelectron spectroscopy (XPS)

To study the chemical composition of the uppermost layer and exposed functional groups, CT_ fun and CT_coating samples, and CT as a reference were analyzed by X-ray photoelectron spectroscopy (XPS, PHI 5000 VERSAPROBE, PHYSICAL ELECTRONICS). All the analyses were conducted using a monochromatic Al Kα source (23.8 W) operated at 20 mA and 15 kV and a spot size of 100 μm, with an energy resolution below 0.5 eV with step interval of 0,1 eV. Survey spectra were acquired at pass energy of 187.6 eV and a total acquisition time of 5 min. The fitting was performed through Casa XPS software. Both survey spectra (0–1200 eV), for the identification and quantification of chemical elements, and high-resolution spectra (C, O regions) for the identification of functional groups were acquired. To ensure compensation for the charge effect, the spectra were referenced by setting the C1s peak of hydrocarbons at 284.80 eV.

2.8. Contact angle

Surface wettability was assessed by contact angle measurements obtained by the sessile drop method: a drop of 10 μl of water was deposited by a syringe on the surface of the samples (CT, CT_coating, and CT_fun). The contact angle was determined by acquiring and processing the images by using Image J software. The measurements were performed twice on each sample. The mean value and standard deviation were calculated and represented.

2.9. Antibacterial evaluation

A commercial strain of the biofilm former pathogen *Staphylococcus epidermidis* (*S. epidermidis*, reference strain ATCC 14990) was obtained by the American Type Culture Collection (ATCC, Manassas, USA) and cultivated in Trypticase Soy Agar (TSA, Merck) at 37 °C until round single colonies were observed; then, 2–3 colonies were resuspended in 20 ml of Luria Bertani broth (LB, Merck) at 37 °C under agitation (90 rpm) till reaching a final concentration of 1×10^5 cells ml^{-1}, corresponding to an optical density (OD) of 0.001 at 600 nm determined by spectrophotometer (Spark, Tecan, Switzerland).

To perform the direct infection, specimens were gently located into 24 multiwell plates and submerged with 1 ml of the above-mentioned bacteria suspension for 24 h at 37 °C; afterwards, bacteria metabolic activity was evaluated by the colorimetric Alamar blue assay (AlamarBlue™, Life Technologies) whereas the number of the viable colonies adhered to the specimens' surface was counted by the CFU method. Briefly, the ready-to-use Alamar solution was added to each well containing the test specimen and incubated for 4 h in the dark; then supernatants were collected and measured via fluorimetric analysis (λex = 570 nm and λem = 590 nm). For CFU count bacteria were detached from specimens' surface by vortex and sonicator (3 times each, 30 s) to perform six-serial 10-fold dilutions as previously described by the Authors [38]; the final number of CFU was calculated as follow:CFU = [(number of colonies × dilution factor)$^{\text{serial dilution}}$] Finally, bacteria morphology was visually checked by scanning electron microscopy (SEM, JSM-IT510 from Jeol). Briefly, after fixation in glutaraldehyde (20 min, room temperature) specimens were dehydrated by the alcohol scale (70–90–100%, 30 min each), treated with hexamethyldisilazane and cover-sputtered with gold prior to collect images at different magnifications.

2.10. Cytocompatibility evaluation

Specimens' cytocompatibility was evaluated towards human mesenchymal stem cells (hMSC). Cells were obtained from ATCC (PromoCell C-12974) and cultivated in low-glucose DMEM (Sigma-Aldrich) supplemented with 15% fetal bovine serum (FBS, Sigma-Aldrich) and 1% antibiotics at 37 °C, 5% CO_2 atmosphere. Cells were cultivated until 80%–90% confluence, detached by a trypsin-EDTA solution (0.25% in PBS), harvested, and used for experiments. To test specimens' ability to support cells' colonization, hMSC were directly seeded onto specimens' surface at a defined density (2×10^4 cells/sample) and cultivated for 24–48–72 hs allowing adhesion and spread. Then, the cells viability was evaluated by means of metabolic activity using the colorimetric Alamar blue assay as prior described: moreover, the morphology of the cells adhered to the specimens' surface was visually checked by phalloidin (ab176759, AbCam, Cambridge, UK) and 4′,6-diamidino-2-phenylindole (DAPI Sigma-Aldrich, Milan, Italy) cytoskeleton and nuclei staining, respectively. Images were obtained by a fluorescent confocal microscope (TCS SP8 LIGHTNING confocal laser scanning microscope from Leica).

2.11. Statistical analysis of data

Experiments were performed in triplicate of each specimen for all the applied assays. The statistical analyses were performed by the one-way ANOVA followed by Tukey's post-hoc analysis, with a significance level set at $p < 0.05$.

3. Results

3.1. UV– vis spectroscopy

UV–Vis spectroscopy was used to detect the presence of the grafted α-TP molecules on the functionalized and coated samples (CT_fun and CT_coating, respectively). The spectrum of the CT sample was taken as a control of the surface before functionalization. Fig. 1a represents the spectra of the CT, CT_fun, and CT_coating samples. The spectrum of the CT sample shows clear interference ripples caused by the titanium oxide layer: a refraction effect occurs between the transparent titanium oxide

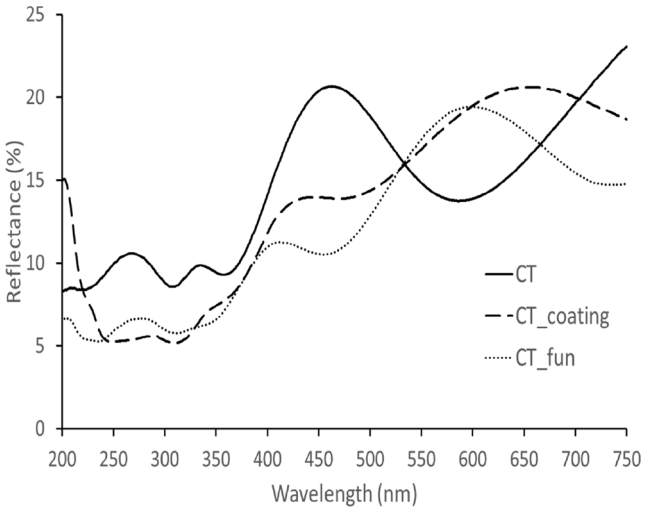

Fig. 1. Reflectance spectroscopy (R%) of the solid samples CT, CT_coating, and CT_fun.

layer and the bulk metal, which creates the typical spectral effect. The spectrum of the functionalized sample (CT_fun) also shows rather pronounced ripples, while for the coated sample the ripples are less pronounced, suggesting that the oxide layer has been masked. All three curves show an upward trend, probably caused by the absorption of UV light by titanium dioxide (TiO_2) [39]. There is a flattening of the spectra of the functionalized and coated samples in the region between 250 and 300 nm, that is the region where the peak absorbance of α-TP occurs: it is most evident for the coated (CT_coating) samples, confirming the presence of a masking coating.

3.2. AFM and Kelvin probe

The use of AFM equipped with a Kelvin probe allowed us to image the presence of the α-TP molecule on the surface of the samples by measuring the electrical potential difference on the border between a chemically treated area and a functionalized or coated one on the same sample (Fig. 2a–d). Fig. 2a shows the macro-optical image of a partially coated sample used for this analysis. Fig. 2b and d show the electric potential of the surface as a 3D image and its absolute value along a horizontal line, respectively. The electric potential difference between the two areas is about 60 mV, with the coating having a lower potential, as expected. The electric potential is homogeneous on the coated area and this result confirms the presence of a continuous layer of α-TP on the surface. Despite the high electric potential difference and the coating visible to the naked eye, there is no difference between the two halves in the AFM image of the topography, as shown in Fig. 2c, which means that the micro- and nano-textures of the CT surface are not covered by the coating. This observation is important if the osteogenic properties of the surface are to be kept intact.

Fig. 3 shows the same images and data in the case of a partially functionalized sample. In this case, the border between the two areas of the sample is not as sharp as it was previously, and it is justifiable considering that a molecular layer of the grafted molecule is expected; a different enlargement has been consequently used for better visualization. Also, in this case, the functionalized surface appears with a uniform electric potential. The electric potential difference between the functionalized and chemically treated areas is about 40 mV, 20 mV less than in the previous case, which can be considered a significant result in terms of the different amounts of α-TP molecules on the surface. Moreover, as Fig. 3a and c show, the difference between the two halves is not visible to the naked eye and by AFM topography imaging. It can be concluded that a thinner layer of the α-TP molecule is grafted on the functionalized samples than on the coated ones, in both cases the grafted molecule forms a continuous layer, and micro-and nano-topography of the surfaces (due to the chemical treatment) is preserved.

3.3. FTIR analysis

FTIR analyses were performed on a drop of a solution of α-TP and on a CT sample, as controls, and on the functionalized or coated samples (CT_fun and CT_coating), respectively. The spectra obtained are shown in Fig. 4. The α-TP spectrum is useful for identifying the molecular groups typical of this molecule.

From an overall comparison of the spectra, it is evident that CT_coating has higher and more defined peaks, corresponding to the α-TP's peaks, which are due to a higher amount of the molecule on the surface, compared with CT_fun. The peaks at 2924 and 2866 cm^{-1}, clearly visible on both CT_coating and CT_fun, are attributed to the asymmetrical and symmetrical stretching vibrations of $–CH_3–$ and $–CH_2–$ in the long alkyl chain of the molecule [40]. The peaks at 1459 and 1376 cm^{-1} are associated with the phenyl skeletal and CH bending, respectively [41]. These peaks are clearly visible on the CT_coating sample, while on the functionalized one (CT_fun) they are not clearly visible, probably due to the sensitivity of the instrument. The peak at 1252 cm^{-1} is attributed to the alkyl CH vibration [42]. This peak is clearly visible in both samples (CT_coating and CT_fun), confirming the presence of the long side chain of the molecule. The peak typical of α-TP, which makes the difference with alpha-tocopherol, is the one at 1093 cm^{-1} attributed to the phosphate group, specifically the stretching band

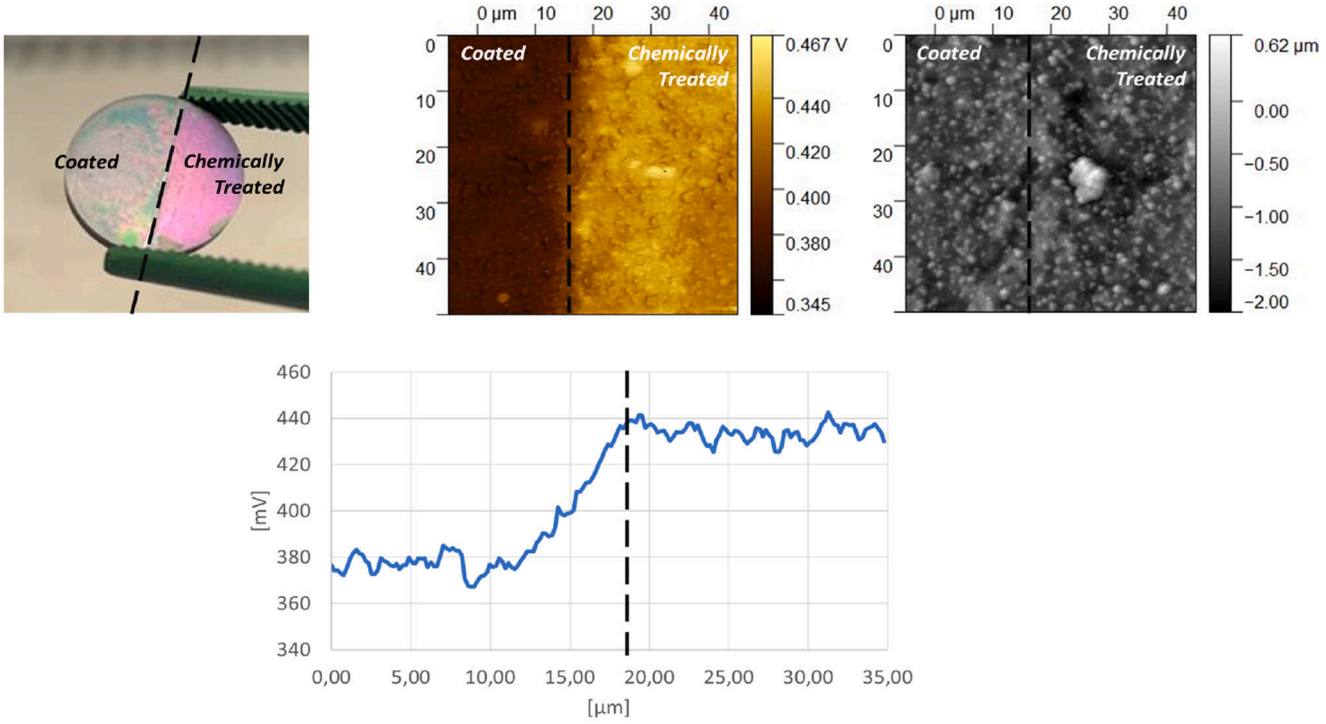

Fig. 2. AFM and Kelvin Probe measurements on a partially coated CT sample: (a) macro-optical image of the sample. (b) Image of electric potential of the sample, measured at the border between the coated and un-coated parts. (c) Topography of the sample (d) Potential difference (in mv) along a horizontal line of the scanned area. The scanned area is the same in b-c-d.

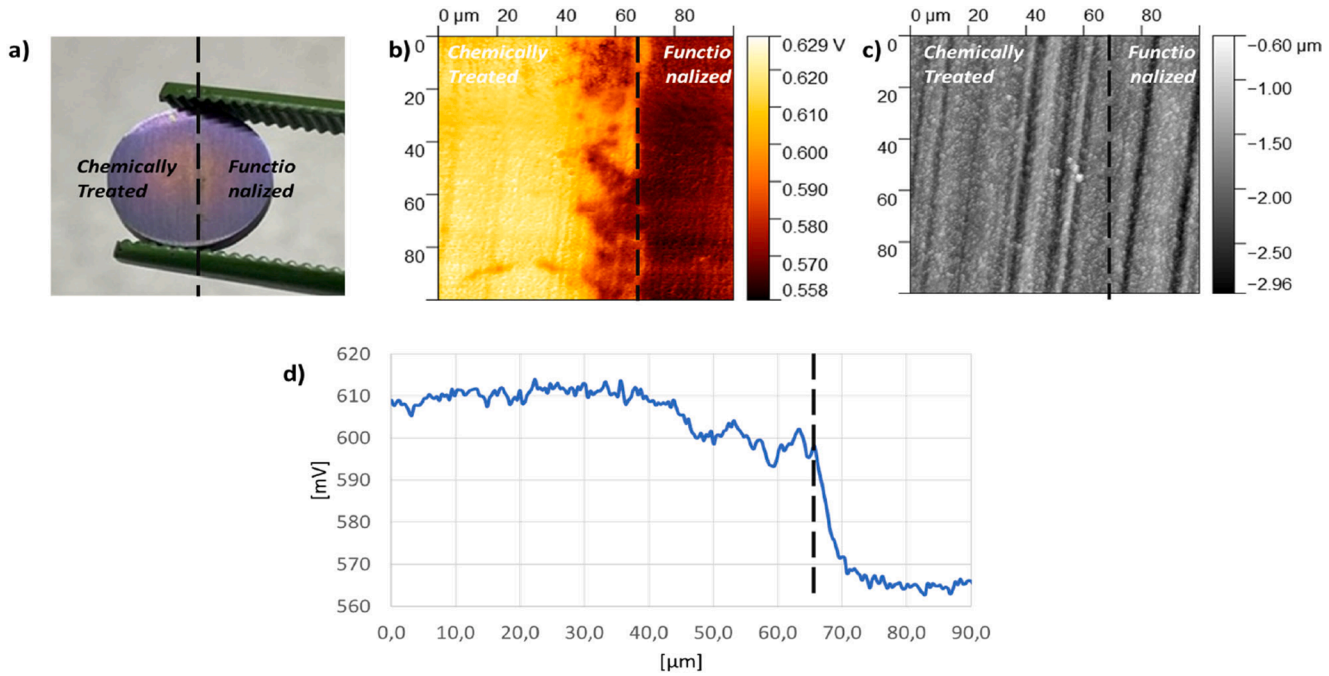

Fig. 3. AFM and Kelvin Probe measurements on a partially coated CT sample: (a) macro-optical image of the sample. (b) Image of electric potential of the sample, measured at the border between the coated and un-coated parts. (c) Topography of the sample (d) Potential difference (in mv) along a horizontal line of the scanned area. The scanned area is the same in b-c-d.

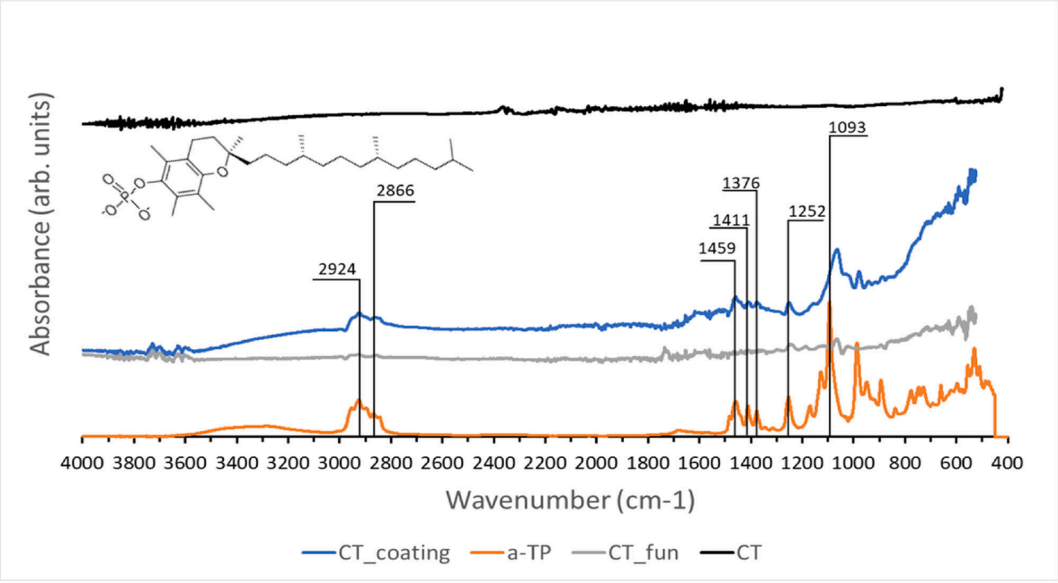

Fig. 4. FTIR analysis of CT, CT_coating, CT_fun, and α-TP.

of -PO_4^{2-} [43]. This peak turns out to be slightly shifted on both the samples, probably due to the formation of a complex with Ca^{2+} ions which are adsorbed on the surface before the grafting of α-TP.

3.4. ζ potential titration curves:

The titration curves of the CT, coated, and functionalized samples (CT, CT_coating, and CT_fun, respectively) are shown in Fig. 5. Although the isoelectric point value (IEP) was not measured, due to measurement limitations, it is derived by interpolation to be in the range of pH 2–3 for the CT and the coated samples. It is due to the presence of functional groups with an acidic chemical reactivity. Both curves exhibit a well-defined plateau for pH values above 5.5, indicating that the acidic groups have a specific acidic strength and completely dissociate above pH 5.5. In the case of CT, the acidic functional groups are bridged hydroxyls of the titanium oxide layer [44]. The lower plateau values of the ζ potential of the coated sample (CT_coating) can be justified by the exposure of negatively charged phosphate groups on the surface. The value of pKa reported in the literature for the complete deprotonation (from -HPO_4^- to -PO_4^{2-}) of the phosphate group of tocopheryl phosphate is around 6 [45]. The obtained curve of CT_coating basically agrees with the literature, even if the pKa seems to be shifted to around 5. In addition, the similar, rather low slope between in the other two samples, the curve is not stable at acidic pH (below pH 4) with a rather high standard

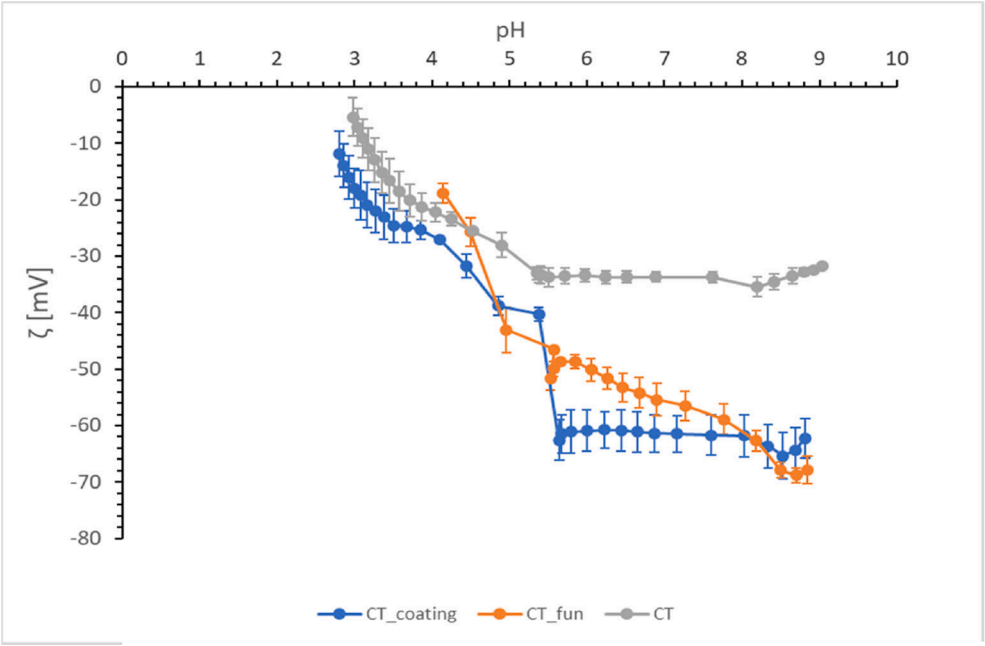

Fig. 5. ζ potential vs pH for CT, CT_coating, and CT_fun.

deviation (data not shown). The steep slope of the curve can be accounted for by the hydrophobicity of the surface evidencing that the hydrocarbon (phytyl) tail of the molecule is mainly exposed outwards. The absence of the plateau in the basic region can be explained by the lack of negatively charged phosphate groups exposed on this surface by α-TP and by a complete covering of the CT substrate and its acidic OH groups. pH 3 and 5 of both CT and CT_coating may be related to the high wettability of the two samples. In fact, water, being strongly adsorbed by hydrophilic surfaces, hardly detaches from it, making slow the replacement by OH groups from the solution. As a result of this process, the ζ potential slightly changes by changing the pH of the solution, above pH5.5, because the functional groups of the surface do not change their chemical state and no ions are adsorbed from the solution.

3.5. X-ray photoelectron spectroscopy (XPS)

XPS analysis was performed on the coated and functionalized samples (CT_coating and CT_fun), and on the control sample (CT) as a reference, to quantify the elements present on the surfaces and their chemical state. The atomic element percentage, as detected in the survey spectra of the different samples, is reported in Table 1 and survey spectra for the three samples are reported in Fig. 6. A large amount of oxygen was detected on the CT sample, confirming the presence of an oxide layer on the surface. The Ti amount is similar for the CT and CT_fun sample, while on the coated (CT_coating) sample, the Ti alloy substrate is not detectable, supporting the previous results (UV–Vis reflectance, KPFM, FTIR) that show the presence of a thicker coating on this sample. A high percentage of carbon is found on the CT since, as a common contaminant, it adsorbs very easily on titanium surfaces, but it grows considerably for CT_coating, with respect to the CT sample, because of the presence of the organic coating, whereas the percentage of oxygen decreases because of the titanium oxide layer is no more detectable. Phosphorous, the element that is characteristic of the α-TP molecule, is present in small amounts on both samples (on CT_fun it is half than on CT_coating) and obviously not present on CT. Calcium is detected on both the modified surfaces in small amounts (CT_fun and CT_coating) as a result of the 24 h immersion in a solution of $CaCl_2$.

Table 1
Atomic percentage of the elements detected on CT, CT_fun, and CT_coating after XPS analysis.

	O	C	Ti	P	Ca	Other
CT	46.9	41.8	10.3	–	–	1.1
CT_fun	33.7	54.9	8	1.2	0.4	1.8
CT_coating	15.7	79.3	–	2.3	0.4	2.3

For the determination of the chemical state and binding energy of the elements, a high-resolution analysis was performed on the oxygen and carbon regions, as shown in Fig. 7. In the O1s region, the CT sample, as we expected, has a clearly visible signal given by the bridged acidic OH groups (around 530.5–531.0 eV) and a lower signal due to the terminal basic OH groups at 531.5–532.0 eV. A large contribution around 530.4 eV attributed to Ti–O bonding is also visible due to the TiO_2 oxide layer [12]. In contrast, the spectrum of the CT-coated sample (CT_coating) is significantly different: the signal attributed to the Ti–O bond has disappeared (in agreement with the absence of Ti in the survey), confirming the presence of a thicker coating. Instead, it shows the signals of the phosphate group at about 531 eV (–P=O) [44] and 532.5 eV (–POH) [46], confirming the findings of the ζ potential and contact angle (see next paragraph) measurements, according to which the ionic, hydrophilic phosphate group is largely exposed on the outermost layer of the coating. On the CT_fun functionalized samples, the presence of the characteristic TiO_2 peak is evident (in agreement with the presence of Ti in the survey), confirming that the α-TP layer is so thin to make the oxide layer still detectable by XPS on the functionalized sample. The region of the OH group has several contributions coming from the acidic OH groups of the titanium oxide layer (around 531 eV), overlapped to the –P=O signal of the phosphate group, and the basic OH groups of the titanium oxide layer, overlapped to the -P-OH signal (around 532 eV). Looking instead at the carbon region, the main signal is at 284.8, which is attributed to the C–C and C–H bonds that are always present on the surface of titanium due to the presence of hydrocarbon contaminants. These chemical bonds are also present in the α-TP molecule and, as expected, the related peak is higher on the coated CT sample (CT_coating). The other two peaks present in the carbon spectra are associated with the C–O (286.3 eV) and C–O–C (286–287 eV) bonds [47]. The spectrum of the functionalized sample (CT_fun) is slightly shifted to the right due to the detection of the C–Ca signal [48]. According to the obtained data, it can be concluded that the result of the functionalization

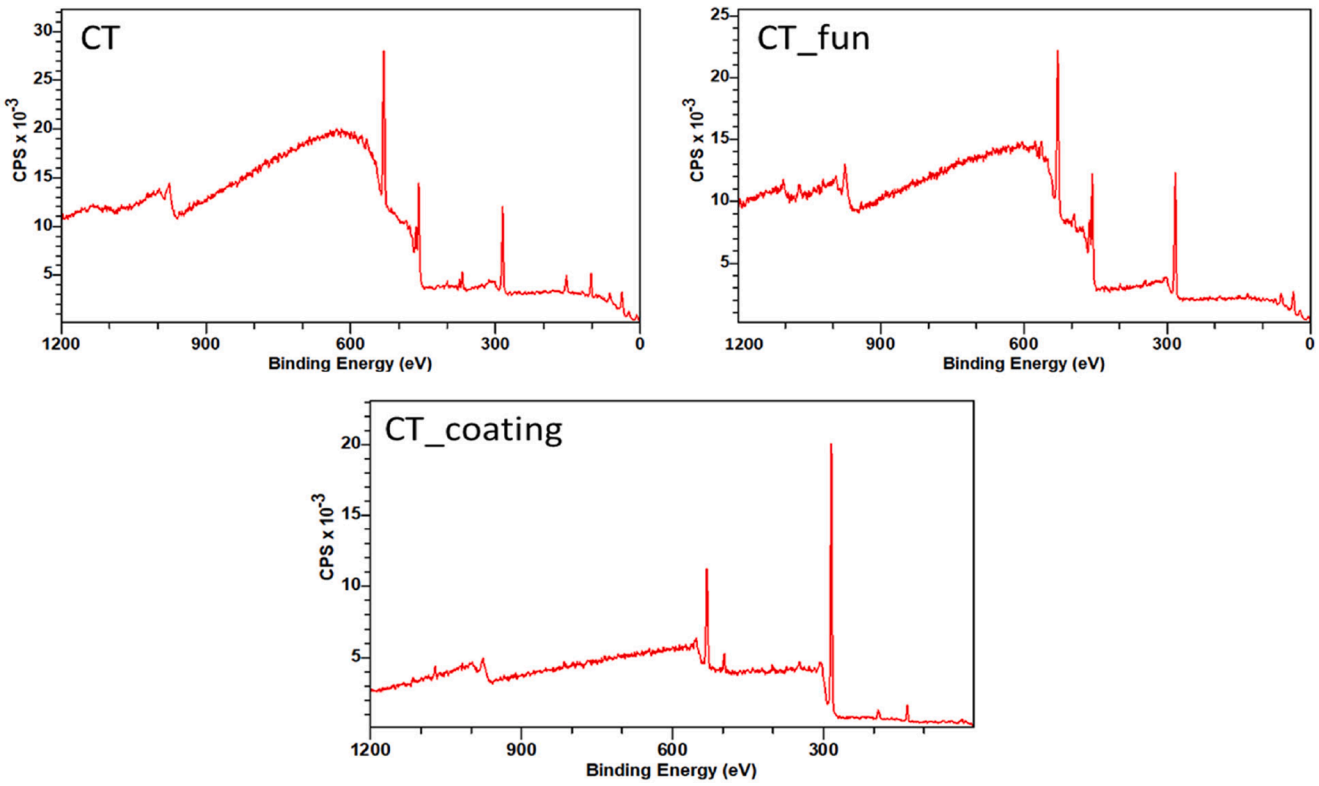

Fig. 6. Survey spectra for CT, CT_fun and CT_coating.

process is the adsorption of Ca^{2+} ions by the acidic OH groups of the titanium oxide layer, linking a molecular layer of α-TP, bonded to the substrate through electrostatic attraction with the phosphate group of α-TP and exposing outwards the hydrocarbon tail. In the case of the coating, α-TP makes a thicker coating (<0.2 μm) exposing phosphate groups on the outermost layer.

3.6. Contact angle

As already reported, CT samples show a significant increase in surface wettability with respect to the polished surface, due to the presence of OH groups and nano-topography of the oxide layer created as a result of chemical treatment [49]. Regarding surfaces with α-TP, the functionalized sample (CT_fun) has a significantly higher contact angle than the coated one (CT_coating) ($p < 0.05$) as shown in Fig. 8. This can be explained by assuming that in the functionalized sample, the α-TP molecules use the phosphate group ($–PO_4^{2-}$) to create a bonding with the previous adsorbed Ca^{2+} ions, thereby exposing outwards the long hydrophobic alkyl chain, in agreement with the previous data. On the other hand, the wettability of the the coated samples (CT_coating) is not significantly different from that of the CT sample ($p > 0.05$), in agreement with the exposition of the hydrophilic phosphate group. Both the CT and CT_coating surfaces can be considered hydrophilic, while the functionalized one is hydrophobic. Wettability is of great importance when considering biological response: it has been shown that osteoblasts are reluctant to adhere to surfaces that have a water contact angle >60° (or a surface free energy <40 mN/m) [50].

3.7. Biological evaluation

3.7.1. Antibacterial activity

Taken into consideration that bone represents the target tissue for the coated and functionalized specimens, *Staphylococcus epidermidis* (*S. epidermidis*) was considered as a reference strain due to its common involvement in orthopaedic and dental implant contamination [51,52]. Moreover, the selected strain (ATCC 14990) is certified as pathogen and biofilm former, so it was selected to verify the ability of the coating to prevent surface colonization and the subsequent 3D biofilm-like formation. Accordingly, specimens were processed with a direct infection of the surface to simulate bacterial colonization of the exposed implant. Results in Fig. 9a shows the metabolic activity of bacteria grown for 24 hs onto mirror-polished and treated samples as control (MP and CT, respectively) and on functionalized and coated samples (CT_fun and CT_coating, respectively). Results are expressed in RFU (relative fluorescent units), and the MP specimens are considered as the control material. The process used to create the α-TP surface layer resulted as a key-point for the molecule efficacy: in fact, only the coating (CT_coating) was effective in reducing the metabolic activity of bacteria in a significant manner in comparison to MP, CT samples, and the functionalized ones (Fig. 9a, $p > 0.05$indicated by #). Such inhibitory activity resulted in a 93(±6) % reduction of bacterial viability (Fig. 9b) when *S. epidermidis* colonies were seeded onto CT_coating surfaces in comparison to the MP control. As a confirmation of the inhibitory activity determined by α-TP after coating, when the number of viable colonies (CFU) adhered to the specimens' surface was counted, a reduction >3 logs was observed between CT_coating and MP control specimens (Fig. 9c, $p < 0.05$ indicated by #). CT_fun prevented bacterial proliferation (the starting infection number is indicated by the dashed line in Fig. 9c), but reduced the final number of ≈1 log, thus failing an irrefutable antibacterial effect. Finally, SEM imaging was used to investigate bacterial morphology and aggregation (Fig. 9d). As expected, from the previous results, the MP and CT surfaces showed a high degree of bacterial colonization and a frequent appearance of 3D biofilm-like aggregates (appreciable in the higher magnification images). On the opposite, the CT_coating surfaces reported a low degree of contamination and only rare aggregates. The CT_fun results as less contaminated than the MP and CT ones, but more colonies (mostly single cells) were detected in comparison with the coated ones. Therefore, SEM imaging basically confirmed the Alamar and CFU results, confirming the very promising efficacy of α-TP deposited by the coating

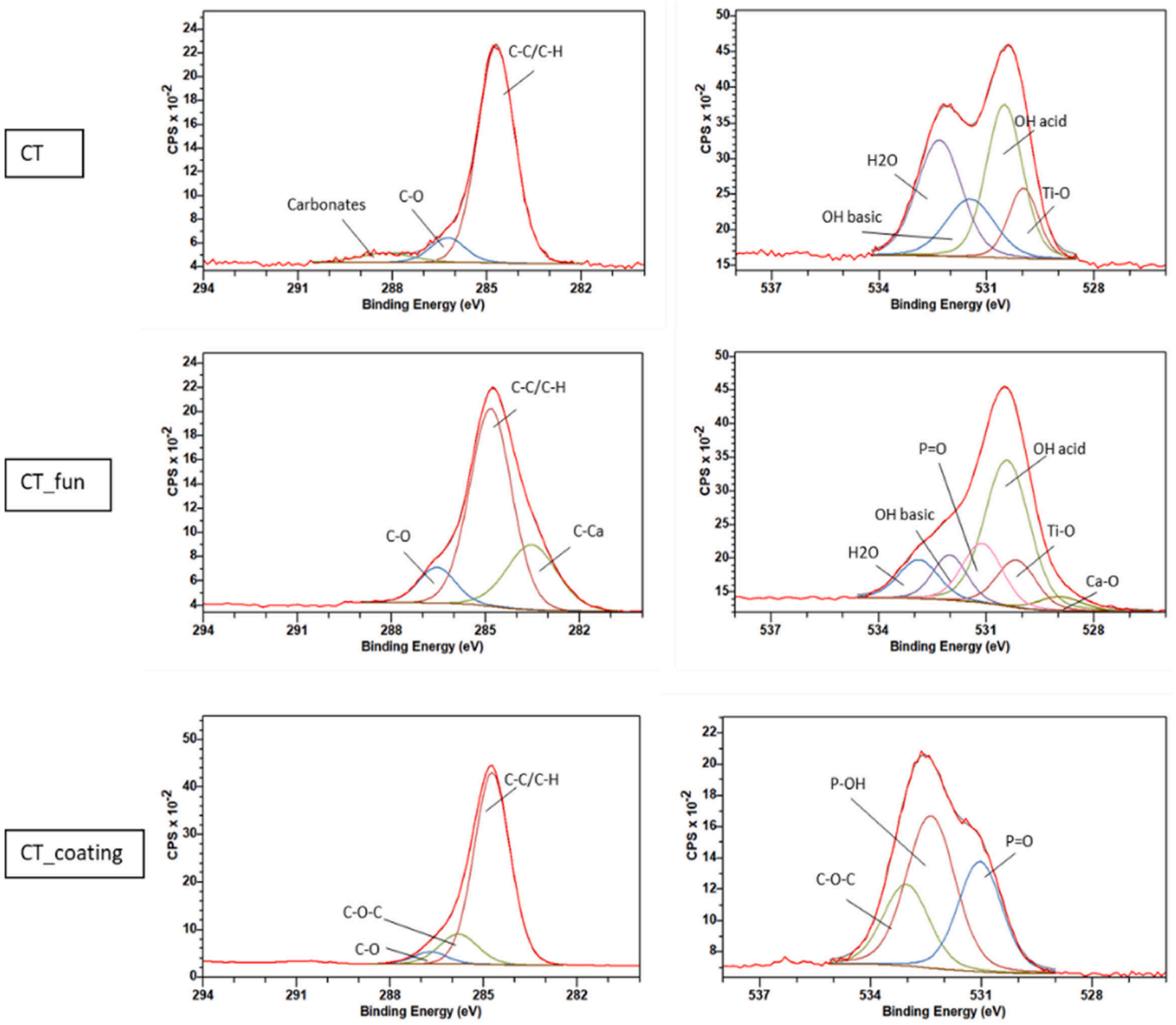

Fig. 7. High-resolution XPS spectra of C and O1s regions of CT, CT_coating, and CT_fun.

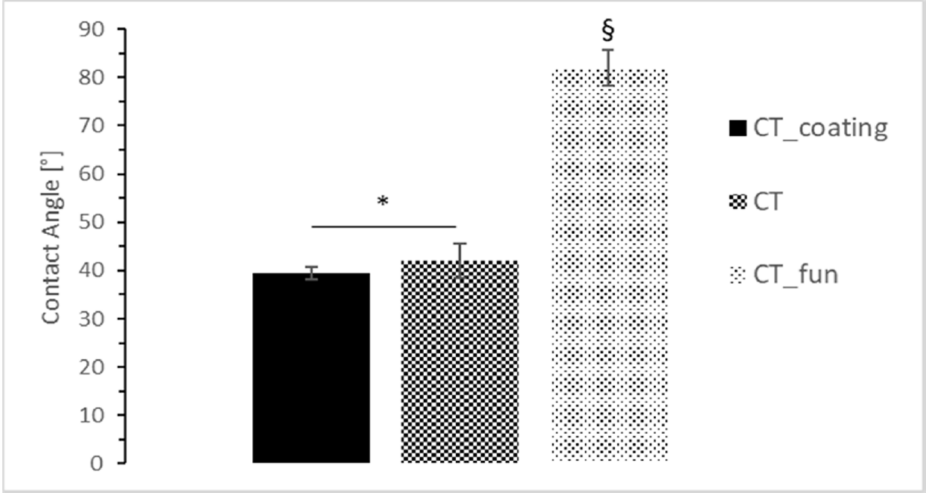

Fig. 8. Contact angles measured on CT and on CT_coating (no significant statistical difference is indicated by *) and on the functionalized samples (CT_fun, $p < 0,05$, indicated by §).

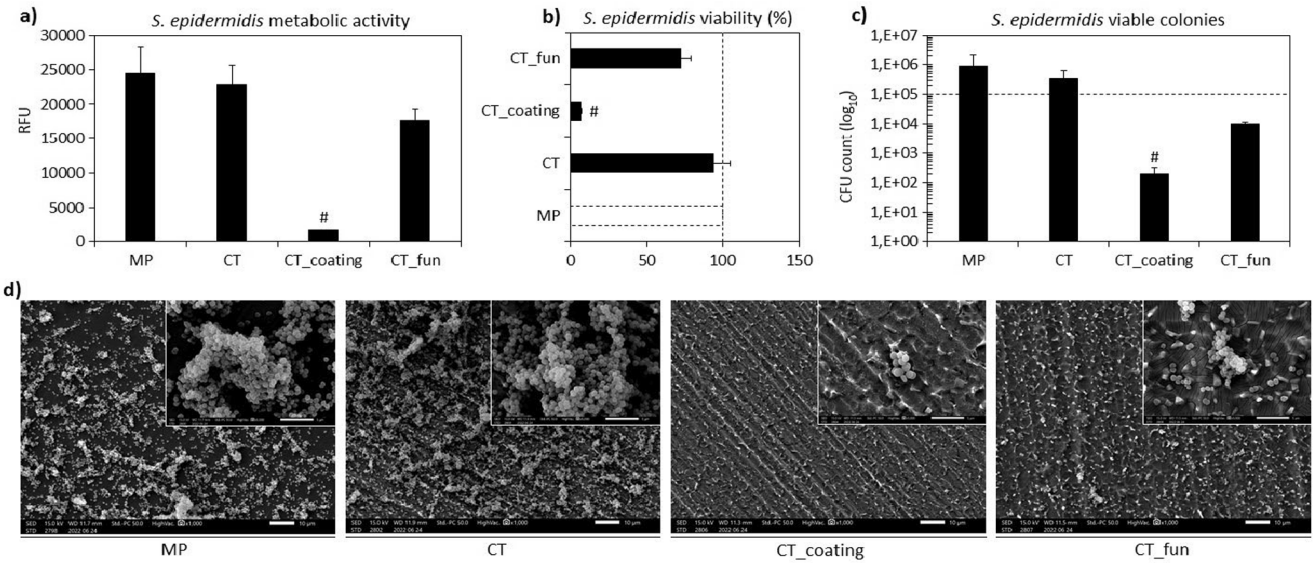

Fig. 9. Antibacterial activity. (a) The α-TP coating method resulted as highly effective by significantly reducing the metabolic activity of adhered bacteria in comparison to the other specimens (#=$p < 0.05$). (b) The efficacy of the coating method determined a viability reduction of 93(±6) % with respect to the MP controls. (c) The count of the viable colonies (CFU) revealed a > 3 log reduction between the CT_coating and the MP controls. (d) SEM images confirmed the lower bacterial colonization degree for the CT_coating surfaces as well as the reduction of biofilm-like 3D aggregates. Bars represent means ± dev.st of replicates = 3. SEM images: low magnification = 1000x, bar scale = 10 μm; high magnification = 5000x, bar scale = 1 μm.

method in preventing bacteria colonization of implantable metal devices.

3.7.2. Cytocompatibility evaluation

Ti-6Al-4V devices are mostly aimed at permanent bone replacement. So, tissue growth in tight contact with the device should be expected after implantation; progenitor and mesenchymal cells play a pivotal role in the formation of such tissue-device connections by firstly migrating to the injured site and then by differentiation into the mature bone lineage [53]. In fact, the first tissue-device sealing is crucial for the correct osteointegration avoiding tissue micro-fracture due to scaffold micro-displacements; therefore, the implanted device should improve or at least do not impar the migration and the following colonization of such cells. Following this principle, human mesenchymal stem cells (hMSC) were used to evaluate the cytocompatibility of the test materials coated or functionalized by α-TP. Fig. 10 shows the viability of hMSC cultured directly onto the surface of controls (MP and CT), functionalized, and coated samples (CT_fun and CT_coating, respectively) after 24

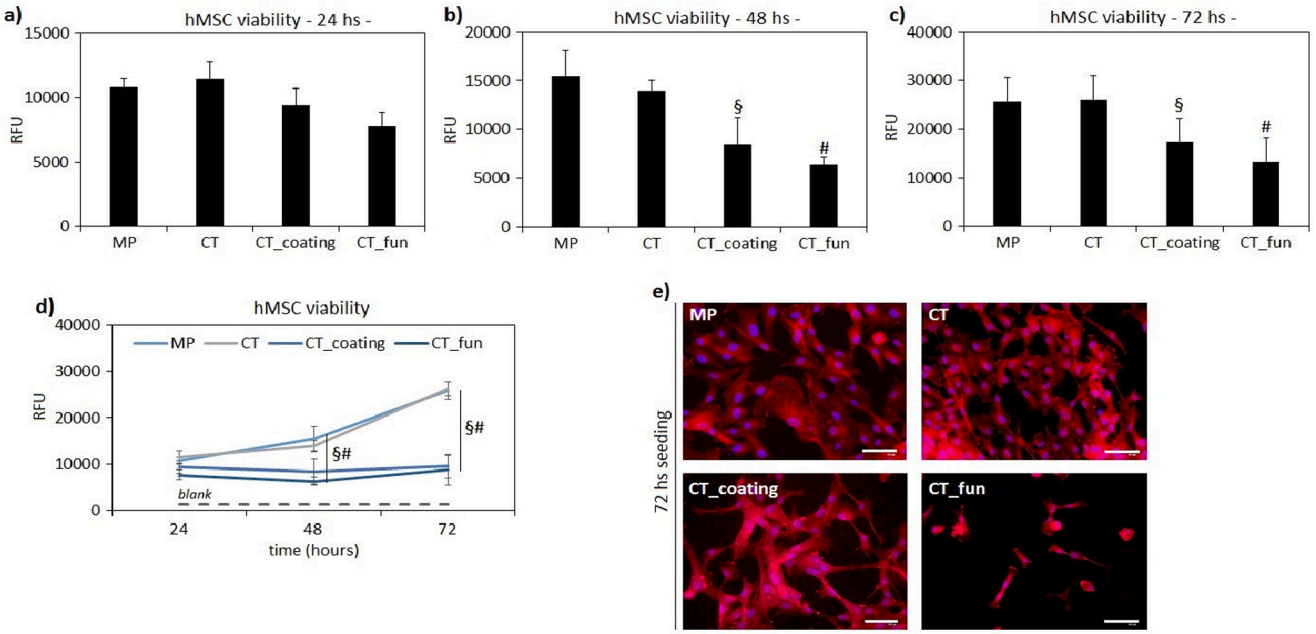

Fig. 10. Cytocompatibility evaluation. (a-c) hMSC metabolic activity was significantly reduced over time by the presence of the α-TP in both CT_fun or CT_coating with respect to MP and CT controls ($p < 0.05$ indicated by § and #). (d) However, results reported as lines in function of time suggested mostly a delayed proliferation rather than a toxic effect since values did not decrease over time in CT_fun and CT_coating. (e) Fluorescent images revealed that cells cultivated onto CT_coating hold a morphology comparable to the MP and CT controls even if with a lower density, whereas cells were mostly round shaped on CT_fun. Bars represent means ± dev.st of replicates = 3. Fluorescence images: red = cytoskeleton (phalloidin), blue = nuclei (DAPI), bar scale = 100 μm.

(Fig. 10a), 48 (Fig. 10b) and 72 h (Fig. 10c) by means of their metabolic activity evaluation that was expressed as RFU. The results showed an increase in viability at the different time points for the control samples (MP and CT), while the cells seeded onto CT_fun and CT_coatin showed a significant decrease in comparison to the controls from day 2 of cultivation (Fig. 10b–c # and § $p < 0.05$ vs MP controls). However, looking at the results reported as lines in function of time in Fig. 10d, it can be speculated that the cells onto the α-TP doped surfaces are not induced to an apoptotic phase, since the values did not decrease with respect to the first time-point of 24 h, as can be expected by a cytotoxic effect. It looks pretty that they are slower to grow with respect to the MP and CT controls where the increase in terms of metabolism is faster (appreciable already at 48 h, Fig. 10b) and continuous over days.

Moreover, an important difference between the coated and functionalized samples can be observed by analyzing the images obtained from fluorescence staining of the cytoskeleton and nuclei (Fig. 10e). The morphology of the cells seeded onto the CT_coated sample resulted as elongated and flat, thus being comparable to the ones adhered and spread onto MP control and CT as well. In fact, the deposition of lamellipodia through the processes of actin filament polymerization and branching is also clearly visible on the coated surface. On the other hand, the cells found CT_fun sample did not display a correct morphology: in fact, they are small, rounded, and not interconnected to each other. These results are in line with what was expected: cells resulted as more prone to adhere to the hydrophilic CT_coating surfaces, whereas, on the opposite, they did not successfully colonize surfaces with a contact angle $>60°$, as it is for the functionalized surfaces of the CT_fun specimens.

So, taken in consideration the aim of this preliminary evaluation aimed at the evaluation of the safety of the doped surfaces, results related to the coating specimens can be considered as promising even if further evaluations are still necessary to verify if the specimens will be able to confirm the same cytocompatibility in a real physiological environment in contact with bone.

4. Conclusions

This paper presents a novel application of α-TP (α-tocopheryl phosphate), a water-soluble form of vitamin E with proven antibacterial properties. The goal was to graft the α-TP molecule onto the surface of chemically treated Ti6Al4V alloy to obtain surfaces for bone contact devices that could actively reduce the risk of bacterial infection. Accordingly, on the CT surface, the molecule was successfully applied both in the form of a grafted molecular layer (functionalization) and as a thin coating (<0.2 μm thick). Physico-chemical characterizations of the functionalized and coated samples were carried out in parallel to study their similarities and differences and to understand which one might be more successful in a future medical application. The studies performed demonstrated the presence of the α-TP molecule as a continuous layer that does not cover the topography of the substrate, thus not altering its pro-osteogenic properties, on both surfaces. It is a thinner and hydrophobic molecular layer on the functionalized surface, while it is thicker, hydrophilic, and rich in phosphate groups in the outermost layer when a coating is formed. The biological tests confirmed very promising antibacterial properties of α-TP and the lack of evident toxic effects in both cases at least at this preliminary in vitro stage in direct contact with human mesenchymal stem cells. In particular, the coating appears to be more promising due to its higher antibacterial effect and cell adhesion. In this sense, the coating can be thought for permanent implant applications, with antibacterial properties. However, a more in-depth study on the stability of the coating and its release kinetics needs to be carried out in the future as well as the delayed cells growth should be considered to render such surfaces more cells friendly.

CRediT authorship contribution statement

Francesca Gamna: Conceptualization, Methodology, Investigation, Data curation, Writing – original draft, Writing – review & editing. **Amanda M. Wiecek:** Investigation, Data curation. **Andrea Cochis:** Investigation, Data curation, Writing – original draft. **Jacopo Barberi:** Investigation, Data curation. **Alessandro C. Scalia:** Data curation, Investigation. **Lia Rimondini:** Project administration. **Silvia Spriano:** Conceptualization, Methodology, Data curation, Writing – original draft, Writing – review & editing, Project administration.

Declaration of Competing Interest

The authors declare that they have no known competing financial interests or personal relationships that could have appeared to influence the work reported in this paper.

Data availability

Data will be made available on request.

References

[1] J. Katić, A. Šarić, I. Despotović, N. Matijaković, M. Petković, Ž. Petrović, Bioactive coating on titanium dental implants for improved anticorrosion protection: a combined experimental and theoretical study, Coatings 9 (10) (2019) pp, https://doi.org/10.3390/coatings9100612.
[2] P. Pesce, L. Canullo, M.G. Grusovin, H. De Bruyn, J. Cosyn, P. Pera, Systematic review of some prosthetic risk factors for periimplantitis, J. Prosthet. Dent. 114 (3) (2015) 346–350, https://doi.org/10.1016/j.prosdent.2015.04.002.
[3] F. Verdugo, T. Laksmana, A. Uribarri, Systemic antibiotics and the risk of superinfection in peri-implantitis, Arch. Oral Biol. 64 (2016) 39–50, https://doi.org/10.1016/j.archoralbio.2015.12.007.
[4] K. Sauer, P. Stoodley, D.M. Goeres, L. Hall-Stoodley, M. Burmølle, P.S. Stewart, T. Bjarnsholt, The biofilm life cycle: expanding the conceptual model of biofilm formation, Nat. Rev. Microbiol. 20 (10) (2022) 608–620.
[5] Z. Khatoon, C.D. McTiernan, E.J. Suuronen, T.F. Mah, E.I. Alarcon, Bacterial biofilm formation on implantable devices and approaches to its treatment and prevention, Heliyon 4 (12) (2018) e01067.
[6] J. Hasan, R.J. Crawford, E.P. Ivanova, Antibacterial surfaces: the quest for a new generation of biomaterials, Trends Biotechnol. 31 (5) (2013) 295–304, https://doi.org/10.1016/j.tibtech.2013.01.017.
[7] H. Chouirfa, H. Bouloussa, V. Migonney, C. Falentin-Daudré, Review of titanium surface modification techniques and coatings for antibacterial applications, Acta Biomater. 83 (2019) 37–54, https://doi.org/10.1016/j.actbio.2018.10.036.
[8] A. Cochis, B. Azzimonti, C. Della Valle, E. De Giglio, N. Bloise, L. Visai, S. Cometa, L. Rimondini, R. Chiesa, The effect of silver or gallium doped titanium against the multidrug resistant Acinetobacter baumannii, Biomaterials 80 (2016) 80–95.
[9] G. Wang, Y. Wan, Z. Liu, Incorporation of antibacterial ions on the micro/nanostructured surface and its effects on the corrosion behavior of titanium, Mater. Lett. 216 (2018) 303–305, https://doi.org/10.1016/j.matlet.2018.01.070.
[10] S. Ferraris, M. Cazzola, G. Ubertalli, E. Prenesti, S. Spriano, Grafting of gallic acid to metallic surfaces, Appl. Surf. Sci. 511 (2020) 145615.
[11] N. Ikeda, S. Fujibayashi, S. Yamaguchi, K. Goto, B. Otsuki, T. Kawai, T. Shimizu, Y. Okuzu, K. Masamoto, Y.u. Shimizu, Y. Takaoka, S. Matsuda, Bioactivity and antibacterial activity of iodine-containing calcium titanate against implant-associated infection, Biomater. Adv. 138 (2022) 212952.
[12] M. Cazzola, S. Ferraris, V. Allizond, C.M. Bertea, C. Novara, A. Cochis, F. Geobaldo, A. Bistolfi, A.M. Cuffini, L. Rimondini, G. Banche, S. Spriano, Grafting of the peppermint essential oil to a chemically treated Ti6Al4V alloy to counteract the bacterial adhesion, Surf. Coat. Technol. 378 (2019) 125011.
[13] R. Jiang, W. Wen, J.M. Wu, Titania nanowires coated PEI/P25 membranes for photocatalytic and ultrafiltration applications, New J. Chem. 42 (4) (2018) 3020–3027, https://doi.org/10.1039/c7nj04628f.
[14] S. He, P. Zhou, L. Wang, X. Xiong, Y. Zhang, Y.i. Deng, S. Wei, Antibiotic-decorated titanium with enhanced antibacterial activity through adhesive polydopamine for dental/bone implant, J. R. Soc. Interface 11 (95) (2014) 20140169.
[15] S. Spriano, S. Yamaguchi, F. Baino, S. Ferraris, A critical review of multifunctional titanium surfaces: new frontiers for improving osseointegration and host response, avoiding bacteria contamination, Acta Biomater. 79 (2018) 1–22, https://doi.org/10.1016/j.actbio.2018.08.013.
[16] S. Rizvi, S.T. Raza, F. Ahmed, A. Ahmad, S. Abbas, F. Mahdi, The role of Vitamin E in human health and some diseases, Sultan Qaboos Univ. Med. J. 14 (2) (2014) 157–165.
[17] F. Gamna, S. Spriano, Vitamin e: A review of its application and methods of detection when combined with implant biomaterials, Materials (Basel) 14 (13) (2021) pp, https://doi.org/10.3390/ma14133691.
[18] L. Capuron, A. Moranis, N. Combe, F. Cousson-Gélie, D. Fuchs, V. De Smedt-Peyrusse, P. Barberger-Gateau, S. Layé, Vitamin E status and quality of life in the

elderly: Influence of inflammatory processes, Br. J. Nutr. 102 (10) (2009) 1390–1394.
[19] F. Renò, V. Aina, S. Gatti, M. Cannas, Effect of vitamin E addition to poly(d,l)-lactic acid on surface properties and osteoblast behaviour, Biomaterials 26 (28) (2005) 5594–5599.
[20] D. Abd, A. Kader, and F. M. Aziz, "Antibacterial Effects of Vitamin E : in Vito Study Antibacterial Effects of Vitamin E : in Vitro Study الحي الكائن خارج دراسة : للبكتريا المضاد هـ فيتامين تأثير," no. January, 2013.
[21] G. Banche, P. Bracco, A. Bistolfi, V. Allizond, M. Boffano, L. Costa, A. Cimino, A. M. Cuffini, E.M.B. del Prever, Vitamin e blended Uhmwpe may have the potential to reduce bacterial adhesive ability, J. Orthop. Res. 29 (11) (2011) 1662–1667.
[22] J.C. Andrade, M.F.B. Morais-Braga, G.M.M. Guedes, S.R. Tintino, M.A. Freitas, I.R. A. Menezes, H.D.M. Coutinho, Enhancement of the antibiotic activity of aminoglycosides by alpha-tocopherol and other cholesterol derivates, Biomed. Pharmacother. 68 (8) (2014) 1065–1069.
[23] B. Mohammadi, H. Shekaari, M.T. Zafarani-Moattar, Synthesis of nanoencapsulated vitamin E in phase change material (PCM) shell as thermo-sensitive drug delivery purpose, J. Mol. Liq. 320 (2020) 114429.
[24] C.H. Lee, D.S. An, S.C. Lee, H.J. Park, D.S. Lee, A coating for use as an antimicrobial and antioxidative packaging material incorporating nisin and α-tocopherol, J. Food Eng. 62 (4) (2004) 323–329, https://doi.org/10.1016/S0260-8774(03)00246-2.
[25] Y. Guo, J. Luo, S. Tan, B.O. Otieno, Z. Zhang, The applications of Vitamin e TPGS in drug delivery, Eur. J. Pharm. Sci. 49 (2) (2013) 175–186, https://doi.org/10.1016/j.ejps.2013.02.006.
[26] A. Ehterami, M. Salehi, S. Farzamfar, H. Samadian, A. Vaez, S. Ghorbani, J. Ai, H. Sahrapeyma, Chitosan/alginate hydrogels containing Alpha-tocopherol for wound healing in rat model, J. Drug Deliv. Sci. Technol. 51 (2019) 204–213.
[27] T.S. Lin, A. Abd Latiff, N.A. Abd Hamid, W.Z.b. Wan Ngah, M. Mazlan, Evaluation of topical tocopherol cream on cutaneous wound healing in streptozotocin-induced diabetic rats, Evid.-Based Compl. Altern. Med. 2012 (2012) 1–6.
[28] F. Gamna, A. Cochis, A.C. Scalia, A. Vitale, S. Ferraris, L. Rimondini, S. Spriano, The use of vitamin E as an anti-adhesive coating for cells and bacteria for temporary bone implants, Surf. Coat. Technol. 444 (2022) 128694.
[29] K. Nishio, N. Ishida, Y. Saito, Y. Ogawa-Akazawa, M. Shichiri, Y. Yoshida, Y. Hagihara, N. Noguchi, J. Chirico, J. Atkinson, E. Niki, α-Tocopheryl phosphate: Uptake, hydrolysis, and antioxidant action in cultured cells and mouse, Free Radic. Biol. Med. 50 (12) (2011) 1794–1800.
[30] A. Bidossi, M. Bortolin, M. Toscano, E. De Vecchi, C.L. Romanò, R. Mattina, L. Drago, M. Rottman, In vitro comparison between α-tocopheryl acetate and α-tocopheryl phosphate against bacteria responsible of prosthetic and joint infections, PLoS One 12 (7) (2017) e0182323.
[31] R.A. Harper, M.M. Saleh, G. Carpenter, V. Abbate, G. Proctor, R.D. Harvey, R. J. Gambogi, A. Geonnotti, R. Hider, S.A. Jones, Soft, adhesive (+) alpha tocopherol phosphate planar bilayers that control oral biofilm growth through a substantive antimicrobial effect, Nanomed. Nanotechnol. Biol. Med. 14 (7) (2018) 2307–2316.
[32] R. Gianello, R. Libinaki, A. Azzi, P.D. Gavin, Y. Negis, J.-M. Zingg, P. Holt, H.-H. Keah, A. Griffey, A. Smallridge, S.M. West, E. Ogru, α-tocopheryl phosphate: a novel, natural form of vitamin E, Free Radic. Biol. Med. 39 (7) (2005) 970–976.
[33] A.B. Lovati, M. Bottagisio, S. Maraldi, M.B. Violatto, M. Bortolin, E. De Vecchi, P. Bigini, L. Drago, C.L. Romanò, Vitamin E phosphate coating stimulates bone deposition in implant-related infections in a rat model, Clin. Orthop. Relat. Res. 476 (6) (2018) 1324–1338.
[34] S. Ferraris, A. Bobbio, M. Miola, S. Spriano, Micro- and nano-textured, hydrophilic and bioactive titanium dental implants, Surf. Coat. Technol. 276 (2015) 374–383, https://doi.org/10.1016/j.surfcoat.2015.06.042.
[35] M. Cazzola, S. Ferraris, E. Prenesti, V. Casalegno, S. Spriano, Grafting of gallic acid onto a bioactive Ti6Al4V alloy: a physico-chemical characterization, Coatings 9 (5) (2019) 1–17, https://doi.org/10.3390/coatings9050302.
[36] S. Spriano, S. Ferraris, E. Vernè, Euro. Patent Specif. 2214732 1 (19) (2013) 1–12.
[37] D. Nečas, P. Klapetek, Gwyddion: an open-source software for SPM data analysis, Cent. Eur. J. Phys. 10 (1) (2012) 181–188, https://doi.org/10.2478/s11534-011-0096-2.
[38] A. Cochis, J. Barberi, S. Ferraris, M. Miola, L. Rimondini, E. Vernè, S. Yamaguchi, S. Spriano, Competitive surface colonization of antibacterial and bioactive materials doped with strontium and/or silver ions, Nanomaterials 10 (1) (2020) 120.
[39] H. Li, S. Yin, T. Sato, Persistent deNOx Ability of CaAl2O4:(Eu, Nd)/TiO2-xNy luminescent photocatalyst, Nanoscale Res. Lett. 6 (1) (2011) 1–4, https://doi.org/10.1007/s11671-010-9750-7.
[40] W. Wainipee, D.J. Weiss, M.A. Sephton, B.J. Coles, C. Unsworth, R. Court, The effect of crude oil on arsenate adsorption on goethite, Water Res. 44 (19) (2010) 5673–5683, https://doi.org/10.1016/j.watres.2010.05.056.
[41] Y.B. Che Man, W. Ammawath, M.E.S. Mirghani, Determining α-tocopherol in refined bleached and deodorized palm olein by Fourier transform infrared spectroscopy, Food Chem. 90 (1–2) (2005) 323–327, https://doi.org/10.1016/j.foodchem.2004.05.059.
[42] A. TermehYousefi, S. Bagheri, K. Shinji, J. Rouhi, M. Rusop Mahmood, S. Ikeda, Fast synthesis of multilayer carbon nanotubes from camphor oil as an energy storage material, Biomed. Res. Int. 2014 (2014) 1–6.
[43] D. Krilov, M. Kosović, K. Serec, Spectroscopic studies of alpha tocopherol interaction with a model liposome and its influence on oxidation dynamics, Spectrochim. Acta - Part A Mol. Biomol. Spectrosc. 129 (2014) 588–593, https://doi.org/10.1016/j.saa.2014.03.087.
[44] P.G. Rouxhet, M.J. Genet, XPS analysis of bio-organic systems, Surf. Interface Anal. 43 (12) (2011) 1453–1470, https://doi.org/10.1002/sia.3831.
[45] M. Birringer, Analysis of vitamin E metabolites in biological specimen, Mol. Nutr. Food Res. 54 (5) (2010) 588–598, https://doi.org/10.1002/mnfr.200900457.
[46] A. Nina Adden, Lara J. Gamble, David G. Castner, Andrea Hoffmann, Gerhard Gross, H. Menzela, Phosphonic Acid Monolayers for Binding of Bioactive Molecules to Titanium Surfaces 22(19) (2008) 8197–8204. doi: 10.1021/la060754c. Phosphonic.
[47] B.V. Crist, Demo version (87 pages) PDF handbooks of monochromatic XPS spectra volume 1 – the elements and native oxides (for Ag-Au), Elements 1 (March) (1999).
[48] G. Riccucci, M. Cazzola, S. Ferraris, V.A. Gobbo, M. Guaita, S. Spriano, Surface functionalization of Ti6Al4V with an extract of polyphenols from red grape pomace, Mater. Des. 206 (2021), 109776, https://doi.org/10.1016/j.matdes.2021.109776.
[49] S. Ferraris, S. Spriano, G. Pan, A. Venturello, C.L. Bianchi, R. Chiesa, M.G. Faga, G. Maina, E. Vernè, Surface modification of Ti-6Al-4V alloy for biomineralization and specific biological response: Part I, Inorganic modification, J. Mater. Sci. Mater. Med. 22 (3) (2011) 533–545.
[50] J.O. Hollinger, AN INTRODUCTION, 2022.
[51] M. Miola, A. Cochis, A. Kumar, C. Arciola, L. Rimondini, E. Verné, Copper-doped bioactive glass as filler for PMMA-based bone cements: morphological, mechanical, reactivity, and preliminary antibacterial characterization, Materials 11 (6) (2018) 961.
[52] R. Sorrentino, A. Cochis, B. Azzimonti, C. Caravaca, J. Chevalier, M. Kuntz, A. A. Porporati, R.M. Streicher, L. Rimondini, Reduced bacterial adhesion on ceramics used for arthroplasty applications, J. Eur. Ceram. Soc. 38 (3) (2018) 963–970.
[53] W. Zhang, N. Wang, M. Yang, T. Sun, J. Zhang, Y. Zhao, N.a. Huo, Z. Li, Periosteum and development of the tissue-engineered periosteum for guided bone regeneration, J. Orthop. Transl. 33 (2022) 41–54.